RSC Advances

PAPER

View Article Online
View Journal | View Issue

Cite this: *RSC Adv.*, 2018, **8**, 33030

In situ approach of cementite nanoparticles encapsulated with nitrogen-doped graphitic shells as anode nanomaterials for Li-ion and Na-ion batteries†

Na Na Li,‡ Zhao Min Sheng,‡* Hao Liang Tian, Cheng Kang Chang, Run Ping Jia and Sheng Han*

Received 28th June 2018
Accepted 18th September 2018

DOI: 10.1039/c8ra05544k

rsc.li/rsc-advances

Novel Fe_3C nanoparticles encapsulated with nitrogen-doped graphitic shells were synthesized by floating catalytic pyrolysis. Due to the short synthesis time and controllable pyrolytic temperature, the diameters of Fe_3C core nanoparticles ranged from 5 to 15 nm (Fe_3C@NGS900 prepared at 900 °C) and the average thickness of N-doped graphitic shells was ~1.2 nm, leading to their high electrochemical performance: specific capacity of 1300 mA h g^{-1} at current density 0.2 A g^{-1}, outstanding rate capability of 939 mA h g^{-1} at 3 A g^{-1}, improved initial coulombic efficiency (Fe_3C@NGS900: 72.1% *vs.* NGS900 (pure graphitic shells): 52%) for lithium ion batteries (LIBs), and impressive long-term cycle performance (1399 mA h g^{-1} maintained at 3 A g^{-1} after 500 cycles for LIBs; 214 mA h g^{-1} maintained at 1 A g^{-1} after 500 cycles for sodium ion batteries).

Because of the fast development of portable electronic devices and hybrid electric vehicles, lithium ion batteries (LIBs)[1–8] and sodium ion batteries (NIBs)[9–16] with high energy/power density, good cycling performance, and lack of memory effects are in ever-increasing need. Due to the low theoretical capacity of carbon materials (graphite: 372 mA h g^{-1}),[8,17–22] optimizing the morphology of graphitic electrode materials has been important to improve specific capacity.[1–7,23,24] On the other hand, chemical doping (*e.g.*, N, S, B, P) is an effective strategy to raise their specific capacity by increasing conductivity or active sites for Li^+ or Na^+ storage.[3,4,25–28] Additionally, metallic compounds (*e.g.*, Fe_3C) have been also introduced into improving electrochemical performance of carbon anodes, because such materials are proposed to activate some components for reversible transformation of the solid electrolyte interface (SEI) and further benefit reversible capacity.[13,16,29,30] Unfortunately, most of them have been prepared by complex methods including tedious synthetic steps or long-time annealing,[6,17–19] from which, it is hard to prepare Fe_3C particles with desirable small sizes.[8,13,15,16] Thus, developing appropriate Fe_3C/C electrode materials still requires further research.

In this work, Fe_3C nanoparticles encapsulated with nitrogen-doped graphitic shells (Fe_3C@NGS) were *in situ* approached from floating catalytic pyrolysis. Due to the short annealing time of the pyrolysis, Fe_3C@NGSs was prepared with controllable sizes. Furthermore, the *in situ* approach led the graphitic shells just grew on the surface of Fe_3C core nanoparticles, which improved electron transfer between the cores and the shells. Thus, such nanoparticles might be a superb electrode material towards high performance applications of LIBs and NIBs.

For preparing the Fe_3C@NGSs with controllable sizes, floating catalytic pyrolysis was carried out to shorten synthetic time: the gas mixture was introduced into quartz pipe furnace, which was set at 700–1100 °C. For a typical experiment, nitrogen (flow rate: 80 L h^{-1}), acetylene (10 mL min^{-1}) and ammonia (100 mL min^{-1}) gases were embedded into iron pentacarbonyl held at 10 °C to form the gas mixture. After the pyrolysis, Fe_3C@NGS was collected at the other end of the quartz pipe. The details of materials characterization and electrochemical measurements can be found in ESI.†

As shown in transmission electron microscope (TEM) images of the prepared Fe_3C@NGSs (Fig. 1a–c and S1a of ESI†), the metallic cores (dark section) are encapsulated with their shell (light section). The XRD results (Fig. 1d) shows the metallic core nanoparticles are Fe_3C. Thus, the sample prepared at 900 and 1100 °C have been marked with Fe_3C@NGS900 and Fe_3C@NGS1100, respectively. However, the sample prepared at 700 °C, which has been marked with FN@NGS700, has been oxidized in air at room temperature, because of its poor graphitic layers. Compared with XRD pattern of Fe_3C@NGS900,

School of Materials Science and Engineering, Shanghai Institute of Technology, Shanghai 201418, China. E-mail: zmsheng@sit.edu.cn; Hansheng654321@sina.com; Fax: +86-21-60873439

† Electronic supplementary information (ESI) available. See DOI: 10.1039/c8ra05544k

‡ N. N. L. and Z. M. S. contributed equally to this work.

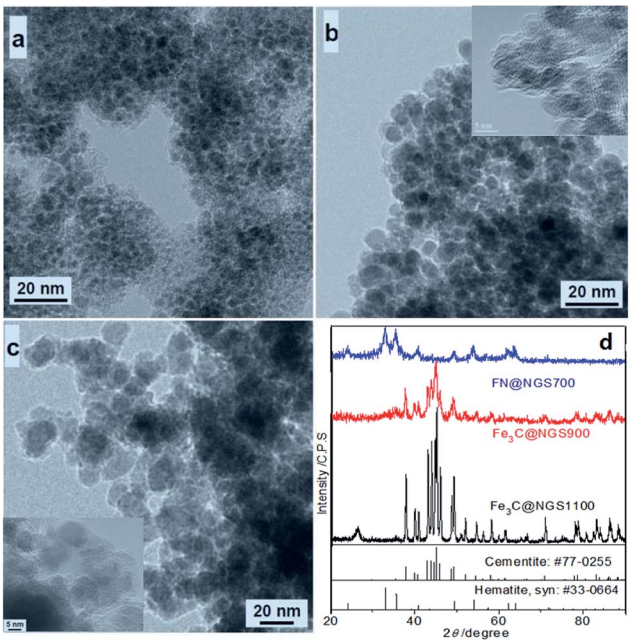

Fig. 1 (a) TEM images of core-shells nanoparticles (FN@NGS700) prepared at 700 °C, TEM and HRTEM (inset) images of nanoparticles (Fe_3C@NGS900) prepared at 900 °C (b) and nanoparticles (Fe_3-C@NGS1100) prepared at 1100 °C (c) and (d) XRD patterns of core-shells nanoparticles prepared at different temperatures.

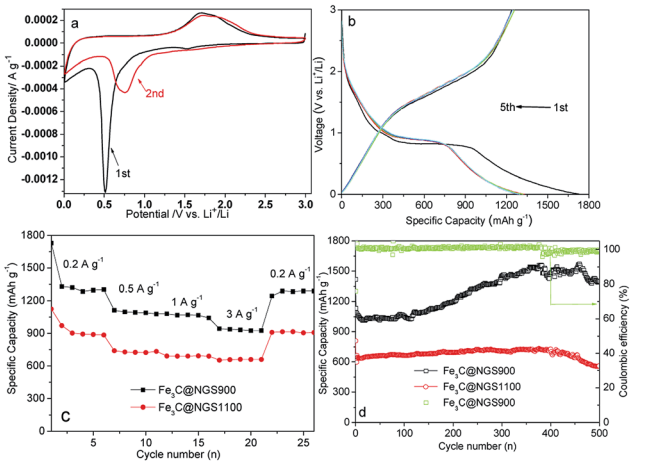

Fig. 2 Electrochemical performance of prepared nanoparticles as anodes for LIBs: CV profile (a) of Fe_3C@NGS900 at a scan rate of 0.1 mV s^{-1} between 0.01–3 V *vs.* Li^+/Li for the 1st–2nd charge/discharge cycles; (b) the galvanostatic charge–discharge profiles of Fe_3C@NGS900; (c) charge–discharge cycling performance of Fe_3-C@NGS core–shell nanoparticles at different current densities from 0.2 to 3 A g^{-1} at room temperature; (d) cycling performance of Fe_3-C@NGS at 3 A g^{-1}.

those peaks of Fe_3C@NGS1100 are much sharper indicating much bigger ferrous cores of Fe_3C@NGS1100. According to the TEM and high resolution TEM (HRTEM) images for Fe_3-C@NGS900 (Fig. 1a–c, S1a, and b†), the diameter of the core nanoparticles is ranged from 5–15 nm and the average thickness of their shells is ~1.2 nm, respectively. Moreover, the spacing of the lattice fringes (Fig. S1a and b†) is ~0.34 nm corresponding to the characteristic (002) peak of graphite implying high graphitization of those shells.[25,28,31] In the HRTEM images, every Fe_3C cores is found to be a single crystal and encapsulated with the graphitic shell. The boundary between Fe_3C cores and N-doped graphitic shells is continuous and distinguished, indicating Fe_3C cores are tightly encapsulated with the graphitic shell.

Fe_3C@NGS samples have been also analyzed by X-ray photoelectron spectroscopy (XPS), which suggests Fe_3C@NGS samples contain Fe, C, O and N atoms (FN@NGS700: C content of 16.3 wt%, Fe content of 54.6 wt%, N content of 1.6 wt% and O content of 27.5 wt%; Fe_3C@NGS900: C content of 26 wt%, Fe content of 67 wt%, N content of 2 wt% and O content of 5 wt%; Fe_3C@NGS1100: C content of 33.7 wt%, Fe content of 52 wt%, N content of 2.3 wt% and O content of 7 wt%). According to XPS results of Fe_3C@NGS900, the weight ratio of Fe_3C cores and graphitic shells is 3.39 : 1. Additionally, the element contents of Fe_3C@NGS samples are different due to their morphology and structure (Fig. 1). Higher O content of FN@NGS700 is because its ferrous cores have been oxidized, and thick-walled graphitic shells (~3 nm) of Fe_3C@NGS1100 leads to its higher C content, as XPS can only measure element contents of surface of samples.

The electrochemical properties of the Fe_3C@NGS-based electrodes have been shown in Fig. 2 and 3. Since FN@NGS700 sample has been completely oxidized, electrochemical properties of ferrous oxide has not been measured. The cyclic voltammetry (CV) curves of Fe_3C@NGS900-based electrode show details of possible lithium storage process. Besides the similar peak (0.5 V) in the initial cycle for the SEI formation, two reduction peaks are located at 0.7 and ~1.5 V, corresponding to the reduction of some SEI components (Li^+ insertion). During the Li^+ extraction process, the corresponding oxidation peaks is found to shift from ~1.7 to ~1.9 V. The almost overlapped oxidation peaks demonstrate good reversibility and cycling stability of core–shell Fe_3C@NGS.[15] As shown in Fig. 2b, the galvanostatic discharge–charge (GDC) profiles of Fe_3C@NGS900 in a voltage range of 0.005–3 V (*vs.* Li^+/Li) exhibits the typical shape of Fe_3C@NGS-based anodes, and Fe_3C@NGS900 delivers initial charge and discharge capacities of 1246.7 and 1729.1 mA h g^{-1}, respectively. The initial columbic efficiency (CE) reaches up to 72.1% which is higher than 52% of pure graphitic shells.[3] For Fe_3C@NGSs electrode, the phenomenon of capacity increment is related to growing reversibly SEI film *via* the decomposition of electrolyte due to the catalysis of Fe_3C.[16,29] From the second cycle, the shape of the discharge profiles changes with respect to that of the first cycle, which may be due to the modification of the SEI film.[12]

The excellent rate capability of Fe_3C@NGS-based anodes have been investigated by testing charge/discharge at current densities of 0.2, 0.5, 1 and 3 A g^{-1} for every 5 cycles (Fig. 2c). At the corresponding rates, the reversible capacities are 1300, 1101, 1062 and 939 mA h g^{-1} for Fe_3C@NGS900; 925, 721, 690 and 663 mA h g^{-1} for Fe_3C@NGS1100, indicating the smaller size of the Fe_3C nanoparticles might enhance their

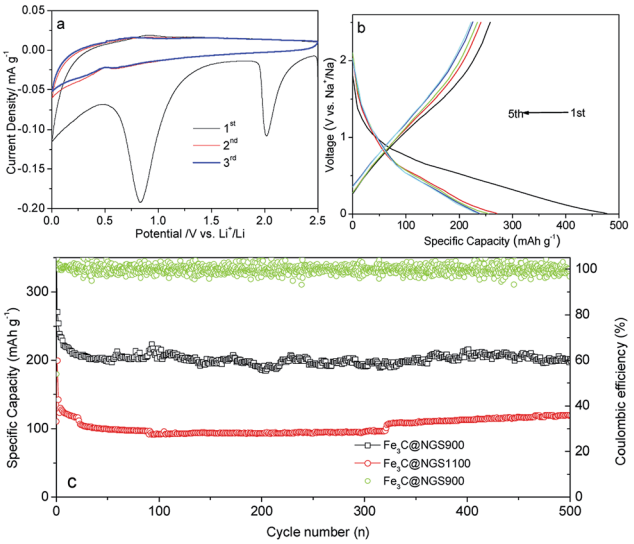

Fig. 3 Electrochemical performance of the prepared nanoparticles as anodes for NIBs: (a) CV profile of Fe_3C@NGS900 at a scan rate of 0.1 mV s^{-1} between 0.01–2.5 V *vs.* Na^+/Na for the 1st–3rd charge/discharge cycles. (b) The galvanostatic charge–discharge profiles of Fe_3C@NGS900; (c) cycling performance of Fe_3C@NGS at a current density of 1 A g^{-1}, and the corresponding columbic efficiency.

electrochemical capability. Compared with reported pure graphitic shells (NGS900 prepared by removing Fe_3C cores of Fe_3C@NGS900),[3] the core–shell nanoparticles (Fe_3C@NGS900) exhibits impressive rate performances (NGS900: 760 mA h g^{-1} at 0.5 A g^{-1}, 620 mA h g^{-1} at 1 A g^{-1} and 340 mA h g^{-1} at 5 A g^{-1}), which might be caused by Fe_3C, as a good conductor of electricity, can effectively improve electrical conductivity of carbon electrode material.[13] Calculated from eqn (1) of ESI,† specific capacity of Fe_3C cores of Fe_3C@NGS900 can be evaluated (1199 mA h g^{-1} at 0.5 A g^{-1} and 1193 mA h g^{-1} at 1 A g^{-1}, respectively). Based on the conversion mechanism for lithium storage, if possible, Fe_3C can store only 1/6 Li per unit (~26 mA h g^{-1}),[15] which is negligible regarding to the high capacity of ~1300 mA h g^{-1}. The specific capacity of Fe_3C is larger than what it should be, which might be resulted from the pseudocapacity on the interface between the material and the electrolyte.[16] For evaluating N doping structure in the graphitic shells, Fe_3C@NGS samples have been prepared with different percent of doping content at 900 °C by introducing ammonia with different flow rates (0, 30, 100 or 500 mL min^{-1}). As a result, Fe_3C@GS900 prepared without ammonia has graphitic shells without N-doping leading to its poor electrochemical performance: at current densities of 0.2, 0.5, 1 and 3 A g^{-1}, its reversible capacities are 575, 492, 458 and 402 mA h g^{-1} (Fig. S4†); the performances of Fe_3C@NGS900 (ammonia flow rate: 100 mL min^{-1}; content of N: 2 wt%) and Fe_3C@NGS900A (ammonia flow rate: 30 mL min^{-1}; content of N: 1.5 wt%) are similar; the sample prepared with ammonia flow rates of 500 mL min^{-1} (FN@NGS900B) was violent oxidized to ferrous oxide in the air. Hence, N doping structure in graphitic shells has been confirmed to enhance diffusion.

The long-term cycling performance of these two electrodes also has been investigated in Fig. 2d. The Fe_3C@NGS-based anode exhibits a favorable reversible capacity, which can reach 1399 mA h g^{-1} after 500 discharge/charge cycles at 3.0 A g^{-1}, showing high capacity retention with CE of ~100%. The capacities of Fe_3C samples increases with cycle number rising (from 120 to 450), which might be attributed to the pseducapacity presented by the Fe_3C.[16]

To better study the kinetic properties of Fe_3C@NGS900 and Fe_3C@NGS1100, Fig. S3 of ESI† shows the Nyquist plots and equivalent circuit obtained from electrochemical impedance spectroscopy (EIS) measurements. Here, R_s represents the ohmic resistance of the battery. Constant phase element (CPE) represents the double layer capacitive reactance between the electrode materials and the electrolyte. The semicircles and straight lines correspond to the electrochemical polarization impedance (R_p) and Warburg resistance (W), respectively.[32] Both the fitted R_s value (5.526 Ω) and R_p value (20.826 Ω) for Fe_3C@NGS900 electrode is much lower than that Fe_3C@NGS1100 electrode (R_s: 8.501 Ω; R_p: 43.665 Ω), indicating the superior redox kinetics in the Fe_3C@NGS900 composite.

In order to study the electrochemical properties of the Fe_3C@NGSs electrode as anodes for NIBs, CV analysis has been carried out at a scanning rate of 0.1 mV s^{-1} between 0.005 and 2.5 V *vs.* Na^+/Na. As shown in Fig. 3a, there are two irreversible reduction peaks around 2.02 V and 0.83 V found during the initial cathodic scan, which could be ascribed to the interaction of Na ions with specific functional groups and the decomposition of electrolyte along with the formation of SEI film on the electrode surfaces.[33,34] For the subsequent cycles, the peak at 2.02 V disappears and the peak at 0.83 V shifts to 0.60 V. For the anodic scan, the main oxidation peak ranging from about 0.47 V to 1.28 V is supposed to be the desodiation reactions.[35] Fig. 3b depicts the GDC curves of the Fe_3C@NGS900-based electrode for the 1st–5th cycle at current density of 0.1 A g^{-1}. The large irreversible capacity in the 1st cycle is attributed to the SEI formation and the irreversible insertion of sodium ion with a relatively large ionic radius.[22,23] Following the first cycle, the charge–discharge curves become more linear which exhibits a higher and more stable CE indicating a stable SEI layer formed in the first cycle.

Meanwhile, cycling performance of Fe_3C@NGS-based anodes for NIBs have been shown in Fig. 3c. In the extended cycling test at 1 A g^{-1}, a reversible capacity 214 mA h g^{-1} of Fe_3C@NGS900 electrode is still maintained after 500 cycles, which is ~2 times the capacity delivered by the Fe_3C@NGS1100 indicating excellent cycling stability of Fe_3C@NGS900. Thus, Fe_3C@NGS-base anodes holds great potential as a promising candidate compared with other carbonaceous anode materials for NIBs (113 mA h g^{-1} at 1 A g^{-1} (modified PFR/C),[36] 188.6 mA h g^{-1} at 0.1 A g^{-1} after 300 cycles (S/C),[33] 150 mA h g^{-1} at 1 A g^{-1} after 200 cycles (S/graphene)[35]).

It is noticed that the excellent electrochemical performance of the prepared Fe_3C@NGSs is apparently ascribed to their novel structure. First, because of *in situ* growing graphitic shells on the surface of Fe_3C during floating catalytic pyrolysis, contact between Fe_3C cores and graphitic shells effectively increases, leading to lower contact resistance and faster electron transfer between the cores and the shells, comparing with traditional

ferrous/carbon composites generated by multistep carbonization approach.[8,13,15,16] Second, due to floating catalytic pyrolysis, sizes of Fe_3C core nanoparticles have been under control (Fe_3C@NGS900: 5–15 nm *vs.* Fe_3C@NGS1100: 15–40 nm). Smaller size of Fe_3C core nanoparticles might increase surface of Fe_3C nanoparticles, leading to distinguished improvement of their electrochemical performance (Fig. 2 and 3), due to active sites for Li^+ or Na^+ storage rising. For comparison, sizes of reported Fe_3C composites have been listed: Fe_3C@C: 60 nm nanoparticles encapsulated with 4 nm carbon shells;[8] Fe_3C@PC: 29 ± 5 nm nanoparticles embedded in 300 nm porous carbon;[16] Fe_3C/C: 300 nm;[13] Fe@Fe_3C/C: 28–58 nm Fe@Fe_3C nanoparticles.[15] Third, introducing Fe_3C to electrode material can promote the reversible formation/decomposition of the SEI film, causing improvement of initial CE (72.1% *vs.* 52%) for LIBs, due to the catalysis function of Fe_3C.[16,29] Fourth, due to *in situ* N-doping (~2 wt%) during their floating catalytic pyrolysis, such defects of the graphitic shells might offer lots channels for fast diffusion of electrolyte and Li^+/Na^+ into those nanoparticles. Fifth, such prepared core–shell nanoparticles have ultra thin-walled graphitic shells (~1.2 nm shown in Fig. 1d), which shorten the diffusion route of ions and electrolyte. All above confirm Fe_3C@NGS900 has novel structure towards the electrochemical applications, compared with the reported works: Fe@Fe_3C/C sample was prepared by sol–gel and carbonization approach, and whether its pure Fe cores was good for Li^+ storage was doubtful;[15] the Fe_3C@C nanoparticles were prepared with no doping carbon shells;[8] the graphitization of carbon structure was doubtful, when ferrous/carbon composites were prepared by polymerization-carbonization of iron phthalocyanine[13] or hydrothermal method-carbonization.[16] Thus, the Fe_3C@NGS900 performs better (1300 mA h g^{-1} at current density of 0.2 A g^{-1}; 939 mA h g^{-1} at 3 A g^{-1}) than many reported ferrous/carbon composite anode materials for LIBs (0.2 A g^{-1}: <382 (Fe@Fe_3C/C),[15] ~480 (Fe_3C/C),[8] 787.9 (Fe_2O_3/C),[5] ~850 (Fe_3O_4/C),[19] 873 (N,S/C),[36] and 881 (Fe_3O_4/C)[9] mA h g^{-1}; 3 A g^{-1}: ~300 (Fe_2O_3@C),[18] ~370 (FeS@C)[21] and ~612 (Fe_2O_3/C)[14] mA h g^{-1}).

Conclusions

In summary, novel Fe_3C nanoparticles encapsulated with nitrogen-doped graphitic shells were synthesized by floating catalytic pyrolysis. Due to the short synthetic time and controllable pyrolytic temperature, the size diameters of Fe_3C core nanoparticles were ranged from 5 to 15 nm (Fe_3C@NGS900 prepared at 900 °C) and average thickness of N-doped graphitic shells was ~1.2 nm. The unique nanoparticles contributed to their high electrochemical performance: specific capacity of 1300 mA h g^{-1} at current density 0.2 A g^{-1}, outstanding rate capability of 939 mA h g^{-1} at 3 A g^{-1}, and improved initial columbic efficiency (Fe_3C@NGS900: 72.1% *vs.* NGS900 (pure graphitic shells): 52%) for LIBs; impressive long-time cycle performance (1399 mA h g^{-1} maintained after 500 at 3 A g^{-1} for LIBs; 214 mA h g^{-1} maintained after 500 at 1 A g^{-1} for NIBs). The excellent electrochemical performance as well as the facile synthesis route makes Fe_3C@NGS promising for application in superior performance LIBs, NIBs and other high-level applications.[13,37–45]

Conflicts of interest

There are no conflicts.

Acknowledgements

This research was supported by Pujiang Talent Project (13PJ1407400) and Funds (14520503100, 15520503400) from Science and Technology Commission of Shanghai Municipality, Fund (LM201740) from Shanghai association for the promotion of scientific and technological achievements, Funds from Shanghai institute of technology (ZQ2018-14, XTCX2017-1) and research fund (project #21306113) from the National Natural Science Foundation of China.

References

1 P. Sengodu and A. D. Deshmukh, *RSC Adv.*, 2015, **5**, 42109.
2 C. Ma, J. Dong, Y. Zhao, J. Li and H. Chen, *Carbon*, 2016, **110**, 180.
3 C. Y. Hong, Z. M. Sheng, M. H. Hu, X. Y. Dai, C. K. Chang, Q. Z. Chen and D. Y. Zhang, *RSC Adv.*, 2016, **6**, 59896.
4 H. Yue, F. Li, Z. B. Yang, J. Tang, X. W. Li and D. Y. He, *Mater. Lett.*, 2014, **120**, 39.
5 C. P. Gu, X. J. Song and S. M. Zhang, *J. Alloys Compd.*, 2017, **714**, 6.
6 J. X. Li, W. W. Wen, M. Z. Zou, Z. G. Huang and L. H. Guan, *Electrochim. Acta*, 2015, **153**, 300.
7 B. Joshi, J. G. Lee, E. Samuel, H. S. Jo, T. Kim and M. T. Swihart, *J. Alloys Compd.*, 2017, **726**, 114.
8 Y. G. Huang, X. L. Lin, X. H. Zhang, Q. C. Pan, Z. X. Yan, H.-Q. Wang, J.-J. Chen and Q.-Y. Li, *Electrochim. Acta*, 2015, **178**, 468.
9 Q. H. Wu, R. F. Zhao, X. Zhang, W. L. Li and M. Chen, *J. Power Sources*, 2017, **359**, 7.
10 Y. Z. Yan, H. L. Tang, J. S. Li, F. Wu, M. Pan, Z. Z. Xie and D. Y. Qu, *J. Colloid Interface Sci.*, 2017, **495**, 157.
11 X. Zhang, S. Han, C. Fan, L. Li and W. Zhang, *Mater. Lett.*, 2015, **138**, 259.
12 Y. L. Tan, K. Zhu, D. Li, F. Bai and P. Zhang, *Chem. Eng. J.*, 2014, **258**, 93.
13 X. Y. Zhao, D. G. Xia, J. C. Yue and S. Z. Liu, *Electrochim. Acta*, 2014, **116**, 292.
14 H. N. Li, X. F. Zhu, H. Sitinamaluwa, S. Q. Zhang and C. Yan, *J. Alloys Compd.*, 2017, **714**, 425.
15 L. Su, Z. Zhou and P. Shen, *Electrochim. Acta*, 2013, **87**, 180.
16 S. H. Chen, J. F. Wu, R. H. Zhou, L. Zuo, P. Li, Y. H. Song and L. Wang, *Electrochim. Acta*, 2015, **180**, 78.
17 Y. Yang, J. Li, D. Chen and J. Zhao, *ACS Appl. Mater. Interfaces*, 2016, **8**, 26730.
18 T. Zhang, C. L. Zhu, Y. S. Shi, Y. Li, S. M. Zhu and D. Zhang, *Mater. Lett.*, 2017, **205**, 10.
19 N. Zhang, C. Chen, X. H. Yan, Y. Huang, J. Li, J. M. Ma and D. Ng, *Electrochim. Acta*, 2017, **223**, 39.

20 X. Qin, H. Zhang, J. Wu, X. Chu, Y. B. He, B. Li and F. Kang, *Carbon*, 2015, **87**, 347.
21 X. Wei, W. H. Li, J. Shi, L. Gu and Y. Yu, *ACS Appl. Mater. Interfaces*, 2015, **7**, 27804.
22 Z. L. Xu, S. S. Yao, J. Cui, L. M. Zhou and J. K. Kim, *Energy Storage Mater.*, 2017, **8**, 10.
23 Y. H. Qu, Z. A. Zhang, K. Du, W. Chen and Y. Q. Lai, *Carbon*, 2016, **105**, 103.
24 G. Maurina, C. Bousqueta, F. Henna, P. Bernierb and B. Simonc, *Chem. Phys. Lett.*, 1999, **312**, 14.
25 Z. M. Sheng, C. X. Guo and C. M. Li, *Electrochem. Commun.*, 2012, **19**, 77.
26 Z. M. Sheng and J. N. Wang, *Carbon*, 2009, **47**, 3271.
27 L. Su, Z. Zhou and P. Shen, *J. Phys. Chem. C*, 2012, **116**, 23974.
28 Z. M. Sheng, X. J. Chang, Y. H. Chen, R. P. Jia and S. Han, *RSC Adv.*, 2017, **7**, 42083.
29 M. Z. Zou, L. L. Wang, J. X. Lia and L. H. Guan, *Electrochim. Acta*, 2017, **233**, 85.
30 J. Zhang, K. Wang, Q. Xu, Y. Zhou, F. Cheng and S. Guo, *ACS Nano*, 2015, **9**, 3369.
31 Z. M. Sheng, M. H. Hu, X. Y. Dai, C. Y. Hong and C. K. Chang, *Microporous Mesoporous Mater.*, 2016, **234**, 224.
32 D. D. Yang, J. Shi, J. H. Shi and H. B. Yang, *Electrochim. Acta*, 2018, **259**, 1081.
33 X. D Shi, Y. X. Chen, Y. Q. Lai, K. Zhang and Z. A. Zhang, *Carbon*, 2017, **123**, 250.
34 W. Li, M. Zhou, H. M. Li, K. L. Wang, S. J. Cheng and K. Jiang, *Energy Environ. Sci.*, 2015, **8**, 2916.
35 X. L. Wang, G. Li, F. M. Hassan, J. D. Li and Z. W. Chen, *Nano Energy*, 2015, **15**, 746.
36 Z. Z. Qiu, Y. M. Lin, H. L. Xin, P. Han, D. Z. Li, B. Yang and J. Xu, *Carbon*, 2018, **126**, 85.
37 Z. L. Yu, S. Xin, Y. You, L. Yu, Y. Lin and J. B. Goodenough, *J. Am. Chem. Soc.*, 2016, **138**, 14915.
38 Z. M. Sheng, C. Y. Hong, X. Y. Dai, C. K. Chang, J. B. Chen and Y. Liu, *J. Nanosci. Nanotechnol.*, 2015, **15**, 3111.
39 B. W. Byles, P. West, D. A. Cullen, K. L. More and E. Pomerantseva, *RSC Adv.*, 2015, **5**, 106265.
40 Z. M. Sheng, C. Y. Hong, N. N. Li, Q. Z. Chen and R. P. Jia, *Electrochim. Acta*, 2018, **259**, 1104.
41 X. Y. Xie, X. J. He, X. L. Shao and S. A. Dong, *Electrochim. Acta*, 2017, **246**, 634.
42 H. Zhang, X. Sun, X. Huang and L. Zhou, *Nanoscale*, 2015, **7**, 3270.
43 X. B. Wang, P. Zhang, J. J. Gao, X. D. Chen and H. Yang, *Dyes Pigm.*, 2015, **112**, 305.
44 Z. H. Liu, D. D. Guan, Q. Yu, L. Xu, Z. C. Zhuang, T. Zhu, D. Y. Zhao, L. Zhou and L. Q. Mai, *Energy Storage Mater.*, 2018, **13**, 112.
45 C. J. Tang, Y. N. Liu, C. Xu, J. X. Zhu, X. J. Wei, L. Zhou, L. He, W. Yang and L. Q. Mai, *Adv. Funct. Mater.*, 2018, **28**, 1704561.